Recent advances in MXene-based nanomaterials for high-performance lithium metal anodes

YANG Jia-lu†, QIAN Yue†, WANG Ke, YUAN Hua-dong, NAI Jian-wei, LIU Yu-jing, WANG Yao, LUO Jian-min*, TAO Xin-yong*

（*School of Materials Science and Engineering*, *Zhejiang University of Technology*, *Hangzhou* 310014, *China*）

Abstract: To tackle the issues of rapid electrode degradation and severe safety issues caused by the uncontrollable growth of lithium dendrites in Li metal anodes (LMAs), two-dimensional transition metal carbides/nitrides (MXenes) with a high electrical conductivity, excellent mechanical properties, and abundant surface functional groups have been used as hosts to induce uniform Li nucleation and alleviate the volume changes, eventually inhibiting the formation of Li dendrites. Recent advances in the use of MXene-based nanomaterials in LMAs are summarized. The problems with using LMAs are first considered, and the ways of using MXene-based nanomaterials for suppressing Li dendrite growth and constructing stable LMAs are then summarized. These include the use of MXenes, MXene-metal hybrids, MXene-carbon hybrids, and MXene derivatives as hosts for the anodes and as additives to modify the electrolyte compositions to increase ionic conductivity and inhibit polymer crystallization. Finally, the challenges and prospects for using MXene-based nanomaterials in next-generation LMAs are briefly discussed.

Key words: Lithium metal anodes; MXene; Dendrites; Lithium metal batteries

1 Introduction

With the rapidly growing requirements for remote monitoring stations, electric vehicles and portable electronic devices, the development of high-energy and cost-effective rechargeable batteries is urgently needed, which propels the exploration and development of new battery materials beyond the conventional lithium (Li)-ion batteries (LIBs)[1–3]. Lithium metal batteries (LMBs) have attracted extensive research attention due to their higher energy densities compared to existing Li-ion technology. For example, the Li-S and Li-O_2 batteries deliver high theoretical specific energies of 2 567 and 3 582 Wh kg^{-1}, respectively, which are much higher than the graphite/Li-CoO_2 (387 Wh kg^{-1}) LIBs[4]. Although Li metal anode (LMA) exhibits exceptional advantages of high theoretical capacity (3 860 mAh g^{-1}) and low redox potential (−3.04 V *vs* standard hydrogen electrode), the Li dendrite formation and unstable solid electrolyte interphase (SEI) causes rapid electrode degradation and short circuit-related safety issues[5–6]. To overcome these issues, a series of strategies including constructing artificial solid electrolyte interface (SEI) layers (Li_3PO_4[7–8], Li_3N[9–10] and LiF-containing SEI[11–13]), modifying electrolyte compositions (solid electrolytes[14–15] and hybrid electrolytes[16–17]), and employing skeleton matrixes to host Li metal (nitride@carbon fiber[18], rGO, porous nickel foam[19], and Cu_3P nanowires[20], etc.) have been adopted. Nanoengineering is a general method to address the technical challenges of LMAs. Some newly developed nanomaterials have emerged as an opportunity to overcome these challenges in recent years.

MXene, as a new family of two-dimensional (2D) layered early transition metal carbides and carbonitrides, was first reported in 2011[21] and has been widely applied in energy storage[22]. The general chemical formula of MXene is $M_{n+1}X_nT_x$ (M, early transition metal including Sc, Ti, Zr, Hf, V, Nb, Ta, Cr, and Mo; X, carbon or/and nitrogen; T_x, surface groups; n=1-4). MXenes are usually synthesized by etching “A” in the precursor of MAX phase, where M

Received date: 2023-01-01; **Revised date:** 2023-07-04

Corresponding author: LUO Jian-min, Professor. E-mail: luo@zjut.edu.cn;
TAO Xin-yong, Professor. E-mail: tao@zjut.edu.cn

Author introduction: †YANG Jia-lu and QIAN Yue contributed equally to this work

is an early transition metal, A is an III or IV A-group element, and X is the C or N[21,23–24]. To date, more than 30 types of MXenes with different compositions, including Ti_3C_2, Ti_2C, Ti_4N_3 and Mo_2C have been successfully synthesized[23,25–26]. In terms of development history, researchers have been committed to improving the synthesis strategies of MXenes from the initial fluoride-based aqueous solutions (such as HF, NH_4HF_2, LiF and HCl mixtures)[27] to electrochemical methods[27–30], an alkali-assisted hydrothermal method[31], water-free etching in polar organic solvents[32], molten salt etching methods[25,33], salt-templated methods[34], thermal reduction method[35], and chemical vapor deposition (CVD) method[36] at present. The MXene synthesis conditions have a significant impact on the morphology, quality, surface groups, and electrochemical performance as well[37–38].

MXenes hold great potential for serving as the hosts of LMAs because of their unique properties. Firstly, MXenes have high conductivity renders them capable of facilitating an efficient electron transfer rate for the electrode. Secondly, MXenes exhibit exceptional mechanical robustness and durability, thereby facilitating the assurance of the electrodes' structural integrity. Thirdly, the presence of lithiophilic functional groups (—O, —F and —OH) on the surface of MXene are able to effectively coordinate with Li ions and induce Li uniform nucleation. Therefore, MXenes could be utilized to enhance the cycle stability and electrochemical performance of LMAs. The first study on MXenes for LMAs was reported in 2017[26]. Since then, MXenes have been extensively used in LMAs. However, there is a shortage of specialized reviews focusing on the progress of MXenes used for LMAs.

In this review, we systematically discuss the latest advances in MXene-based nanomaterials in state-of-the-art LMAs. In the first section, we discuss the technical challenges of LMAs from 3 aspects: the intrinsic features of Li negative electrode, the growth of Li dendrites, and the SEI formed on LMAs. In the second section, we introduce 3 kinds of modification strategies, including designing MXene-based LMA hosts, constructing MXene-based artificial SEI films and modifying MXene-based electrolyte additives (Fig. 1). Specifically, MXene-based hosts are divided into 3 parts: MXenes, MXene-based hybrids (MXene/metal hybrids, MXene/carbon hybrids, and MXene/oxides hybrids) and MXene derivatives. Finally, an overview of future challenges and opportunities of MXene-based nanomaterials for LMBs are briefly discussed.

2 The technical challenges of lithium metal anode

Lithium, located at the top of alkali metals in the periodic table. As such, it has the smallest metal atomic radius, the lightest metal density (0.53 g cm^{-3}), the lowest redox potential, a low melting temperature, and exceptionally high atomic mobility of all metals-metals[39]. All these properties endow LMBs to exhibit sufficient energy density and power performance[40–42]. Nevertheless, the LMBs experience volume expansion during the cycle, which is highly correlated with dendrite growth and unstable SEI[43]. In this context, uncovering and comprehending the mechanisms of dendritic nucleation and growth, as well as the composition of SEI film, aids in the rational design of high-performance LMBs.

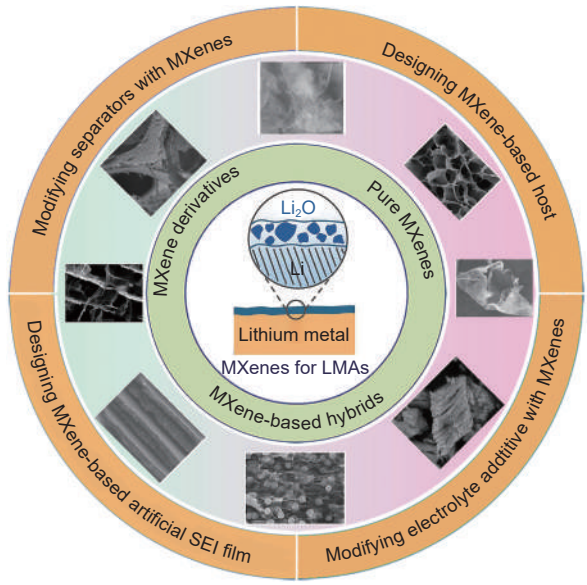

Fig. 1 Schematic diagram of the applications of MXene-based nanomaterials for lithium metal anodes

2.1 Infinite volume changes of Li metal anode

For Li metal anode, due to its hostless nature, the volume expansion during operation is infinite, which is much greater than that of intercalated anodes (~ 10% for graphite), and alloy-type anodes (~ 400% for Si)[41]. Additionally, porous Li formed by dendrite growth causes a greater volume change issue during plating and stripping processes. Regrettably, the capacity degradation of lithium metal batteries is due to the absence of a specific host to trap and restrain Li depositions, resulting in an unstable electrode interface, internal stress fluctuation, and the electrical disconnected Li metal[43].

2.2 Growth of Li dendrites

Lithium tends to form dendrites on the anode current collectors[44]. The growth of dendrites incessantly consumes electrolytes and punctured the separator, which causes an irreversible and permanent loss of capacity, short circuits, as well as potential safety problems[6,45–46]. Lithium dendrites involve in 2 processes: nucleation and growth. So far, 4 models, including the space-charge model, deposition and dissolution model, heterogeneous nucleation model, and stress-driven dendrites growth model, have been proposed to describe the formation and growth of dendrites.

The space-charge theory proposed by Chazalviel et al.[47] emphasizes that the concentration of anions close to the negative electrode decreases when lithium ions are rapidly deposited in a dilute solution. The consumption of Li ions in the near-surface area of the electrode will generate a huge spatial charge and electric field at the electrode/electrolyte interface, eventually induce lithium dendrite formation. The initial time of dendrites growth was named as Sand's time. It has been confirmed that augmenting the Li-ion mobility or reducing the effective current density could lead to an increase in Sand's time[48]. The thermodynamically and kinetically process of heterogeneous nucleation was proposed by Ely et al. through numerical simulation[49]. In this theory, the initial stages of lithium-ion deposition is a heterogeneous nucleation process, including: lithium ions gaining electrons and Li depositing on current collectors. The nucleation of lithium will be affected by the topography and roughness of current collectors. The morphology and uniformity of the initial deposited lithium will directly influence the subsequent lithium metal deposition behaviors and morphology, eventually affecting the formation and growth of lithium dendrites. The growth of Li dendrites could be dramatically suppressed if the Li nuclei are stably established, and the growth rate remains constant until the final form. The deposition and dissolution model reveal that the lithium is extruded through the resulting holes on the protective film broken by the mechanical stress at certain points and grows in the form of whiskers[50]. The stress-driven dendrites growth model was proposed by Jiang et al., namely undesirable filamentary Li dendrite growth is originated from plating induced compressive stress, surface passivation by the SEI, and the presence of subsurface planar defects during Li plating/stripping process. In this case, Li dendrites could be suppressed through effective control of stress[51].

By manipulating the Li nucleation and growth, it is possible to regulate and manage the growth of Li dendrites to achieve a planar morphology, as suggested by these models.

2.3 The SEI on Li metal anode

The properties of the solid-liquid interface have important effects on the charging and discharging efficiency, energy density, power density, service life, safety, self-discharge performance and other characteristics of lithium metal batteries. The solid-electrolyte interphase (SEI) was first defined by Peled in 1979 as a result of irreversible reactions between lithium and non-aqueous liquid electrolytes. This phenomenon is attributed to the ultrahigh chemical reactivity of Li, which leads to the creation of an ionic-conductive but electronic-insulating layer[52–53]. The prevailing depiction of the SEI configuration is the mosaic model. This model assumes that the insoluble reduction products formed by the electrolyte are mosaicked with each other, while lithium ions are in different phases. The boundary between migrations indicating the surface is not homogeneous[54]. Our

groups use Cryo-TEM technology to demonstrate the existence of this model[13].

Researching the SEI film's composition is important because of the crucial role of SEI in influencing the overall performance and safety of LMBs. Experimental and simulation studies have shown that SEI of LMAs comprises degraded inorganic salt, salts/anions such as PF_6^-, $CF_3SO_3^-$, Li_3N, Li_2CO_3, $NS(O_2CF_3)_2^-$, $C(SO_2CF_3)_3^-$ and LiX (X = F, Cl etc.), and reduction products of organic solvents such as $(CH_2OCO_2Li)_2$, $CH_3CH(OCO_2Li)$, CH_2OCO_2Li, CH_3OLi CH_3OCO_2Li, HCOOLi[49–59]. However, a practical SEI is often uneven with poor mechanical performance, which reduces charge and discharge efficiency, increases internal resistance, cause inferior electrochemical performance. Therefore, building a stable (electrochemical and mechanically) SEI is critical.

3 The application of MXene in Li metal anodes

During the Li plating and stripping process, promoting uniform Li deposition is crucial to achieving stable and high-performance LMAs. Extensive materials have been developed to obtain dendrites-free LMAs to date, in which functionally ionic/electronic conductive materials (e.g., carbon nanomaterials[60–62], metal foams[63], and conductive polymers[64]) occupy an important position. By comparison, MXenes exhibit good metallic conductivity, impressive mechanic properties, tunable surface chemistry and rapid ion diffusion ability. All these properties have endowed MXenes with great potential in the applications for advanced LMAs. On the one hand, the high electronic conductivity and fast ion transfer rate of MXenes with abundant functional groups could not only promote uniform Li deposition, but also deliver fast electrochemical kinetics, which suppresses the growth of dendrites effectively. Moreover, the remarkable mechanical properties and facile assembly characteristics of 2D MXenes make them promising candidates for processing into diverse 3D hosts for metal anodes, which could effectively mitigate the volume changes.

3.1 Designing MXene-based hosts for lithium metal anodes

The LMAs exhibit a notable and boundless alteration in volume due to their characteristic of lacking a host, which may damage the SEI film, form lithium dendrites, comsume electrolytes, and reduce the Coulombic efficiency during the repetitive lithium plating and stripping procedure[65]. Designing a proper host for the Li-metal anode would be a great strategy to address these issues. MXenes exhibit excellent mechanical strength and good mechanical flexibility, which could alleviate volume fluctuation during cycling. Besides, MXenes exhibit exceptional metallic conductivity, high Li-ion diffusion coefficient, and versatile surface groups for regulating the electric field distribution, minimizing polarization, and facilitating homogeneous Li nucleation and deposition. Considerable research has been directed towards the utilization of MXene-based nanomaterials for constructing the host of lithium metal anodes since 2017. Efficient LMA hosts include not only MXenes themselves, but also hybrid nanomaterials derived from MXenes and MXene derivatives.

3.1.1 MXene

Yang's group[66] was the first to corroborate the MXenes as the effective Li hosts. They used a roll-to-roll mechanical approach to fabricate Ti_3C_2 MXene (graphene, BN)-metallic lithium film. The synthetic procedure comprised 2 steps as illustrated in Fig. 2a. Initially, the Ti_3C_2 MXene, graphene, or boron nitride nanosheets was subjected to rolling with a lithium plate to achieve elongation. Subsequently, the hybrid plates underwent folding to augment the layer count and obtained a pliable plate with a smooth surface (Fig. 2b-c). The composite anode exhibited fast electron and Li-ion transportation owing to the presence of nucleation sites and the highly conductive networks of MXene (Fig. 2d). Regrettably, the cycle life of this anode was not satisfactory. To this end, Yang's group produced the parallelly aligned MXene layers (PA-MXene) through a simple self-assembly procedure in 2019[67]. The morphology and direction of lithium nucleation and growth on the horizontal plane

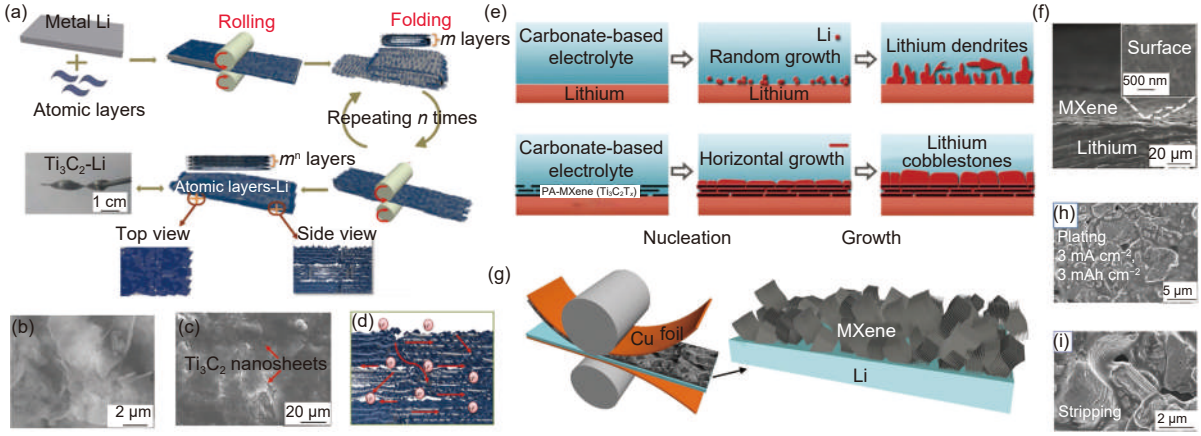

Fig. 2　(a) Schematic illustration of the synthesis of Ti_3C_2 MXene (graphene, BN)-lithium films[66]; (b) SEM image of the Ti_3C_2-Li composite anode[66]; (c) Cross-sectional SEM image of the Ti_3C_2-Li composite anode[66]; (d) Schematic showing the sufficient transport pathways for electron and Li-ion in Ti_3C_2-Li composite anode[66]; (e) Schematic illustration of lithium plating on bare lithium and parallelly aligned MXene (PA-MXene) layers[67]; (f) Typical SEM images of PA-MXene layers on lithium. Inset in (f) is the top view of PA-MXene[67]; (g) Two-side press of MXene stacks onto a thin Li host[69]; (h) SEM images of the ILC-Li electrode upon plating at 3 mA cm^{-2} and 3 mAh cm^{-2}[69]; (i) SEM images of the ILC-Li electrode upon stripping at 3 mA cm^{-2} and 3 mAh cm^{-2}[69]. Reprinted with permission

were efficiently directed by the parallel alignment of MXene ($Ti_3C_2T_x$) layers (Fig. 2e-f). As a result, the cycle life of this material was significantly increased, reaching up to 900 h.

Subsequently, the morphological configuration of MXene nanosheets has undergone continuous development towards structures with low curvature. This modification provides additional internal space for expansion, which effectively mitigates physical strain and preserves structural integrity under high current density. For example, in 2022, Yang and colleagues fabricated sine-wave analogous MXene ($Ti_3C_2T_x$) (SWA-MXene) layers through the self-assembly of MXene layers onto the metallic coil, followed by drying at room temperature[68]. The composite anode relied on its unusually low-curvature construction to effectively eliminate the tip-induced nucleation effect on the surface of SWA-MXene electrodes by uniforming the lithium ions and electric field distribution and lowing the Li-ion concentration gradient. As a result, this anode exhibited a deep plating-stripping capacity of up to 40 mAh cm^{-2}, a long life of up to 1 250 h, and a low nucleation overpotential.

Several studies indicated that when enlarge its interlayer spacing, the expanded MXene exhibited superior ionic and electronic conductivity, as well as excellent volume tolerance, compared to their original MXene nanosheet counterparts. Based on this background, Niu's groups[69] developed an interlayer-calated thin Li metal (ILC-Li) electrode (Fig. 2g-i). The 2D lamination configuration of this composite electrode provided a significant amount of available space, resulting in the overpotential of about 120 mV after 2 200 h at a high current density of 10 mA cm^{-2} and a high capacity of 10 mAh cm^{-2}. Furthermore, the vertically aligned MXene nanosheet arrays could augment conductivity and address the volumetric challenges associated with lithium metal anodes. In contrast to a horizontal structure, a vertical structure offered a greater volume for Li-ion transport, superior mechanical flexibility, and improved electronic conductivity. For this, Yang and Gong[70] utilized an ice template-assisted blade coating technique to fabricate host electrodes consisting of vertically aligned arrays of $Ti_3C_2T_x$ nanosheets (v-$Ti_3C_2T_x$) in a facile manner, as illustrated in Fig. 3a. As depicted in Fig. 3b, the synthesized v-$Ti_3C_2T_x$ was comprised of nanosheet arrays that were vertically aligned, with a gap width of approximately 15 mm (Fig. 3c) and a thickness of approximately 40 mm (Fig. 3d). A full cell constructed with $LiFePO_4$ (1.8 mAh cm^{-2}) cathode and lithiated Li@v-$Ti_3C_2T_x$ anode exhibited specific capacities of 135 mAh g^{-1} and 120 mAh g^{-1} at the rates of 1 and 2 C, much higher than Li@h-$Ti_3C_2T_x$ electrodes

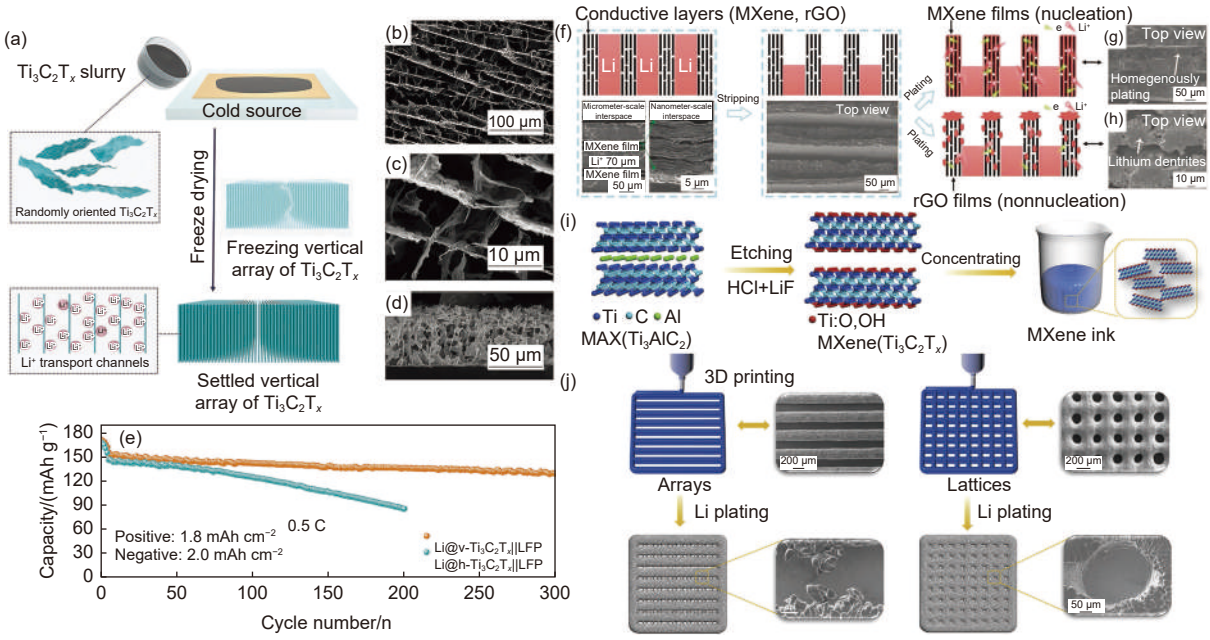

Fig. 3 (a) The synthesis schematic diagram of v-$Ti_3C_2T_x$ electrodes[70]; (b-c) Top view SEM image of v-$Ti_3C_2T_x$ electrodes[70]; (d) Cross-section SEM image of v-$Ti_3C_2T_x$ electrodes[70]; (e) Coulombic efficiencies of v-$Ti_3C_2T_x$ and h-$Ti_3C_2T_x$ electrodes at 1.0 mA cm^{-2} for 1.0 mAh cm^{-2}[70]; (f) Schematic illustration of the stripping and plating states of perpendicular MXene-Li and rGO-Li arrays. The left bottom in a) is the SEM images of as-prepared perpendicular MXene-Li arrays. The middle bottom in panel (a) is the SEM image of perpendicular MXene-Li arrays after lithium stripping for 20 mAh cm^{-2}[71]; (g) Top view SEM images of perpendicular MXene-Li arrays[71]; (h) Top view SEM images of rGO-Li[71]; (i) Scheme of the fabrication of $Ti_3C_2T_x$ MXene and a high-concentration MXene ink (~ 300 mg mL^{-1})[75]; (j) Scheme of 3D printing MXene arrays and lattices to guide the nucleation and growth of lithium[75]. Reprinted with permission

(Fig. 3e). Similarly, Yang's groups[71] developed a brand-new diversified perpendicular MXene-Li array by ice template-assisted blade coating method. Fig. 3f shows the stripping/plating behaviors of Li on the perpendicular MXene-Li arrays. Taking advantage of the tunable MXene walls and space, and flexible structure, the growth of lithium was observed to occur predominantly on the top surface of the arrays, as opposed to within the gaps of the reduced graphene oxide (rGO) structure (Fig. 3g-h). As such, this electrode could be stable under the high-rate capability of up to 20 mA cm^{-2}.

Additive manufacturing technology, commonly referred to as 3D printing, is a nascent technology that could be used to produce a wide range of three-dimensional objects and intricate structures using appropriate inks[72]. The favorable viscosity and shear-thinning rheological behavior of MXene inks makes 2D MXene nanosheets more suitable for being incorporated into 3D architectures through printing[73–74]. For instance, Yang's groups[75] used extrusion-type 3D printing successively developed a highly concentrated MXene ink (Fig. 4i). In the 3D printing arrays, lithium was grown towards the cobblestone rather than dendrites (Fig. 3j). Remarkably, 3D printing MXene (3DP-MXene) arrays-Li delivered a stable capacity of 111.1 mAh g^{-1} at 30 C. From the above discussion, it could be inferred that MXene arrays with abundant interspaces homogenized both lithium-ion flux and electric field, thereby effectively suppressed the formation of lithium dendrites and exhibited admirable electrochemical performance.

As summarized above, the MXene-Li composite anodes could be produced using mechanical rolling, blade coating, and electro-deposition methods. During the assembly process, MXene experiences restacking problems that significantly impact its performance and limit its potential applications. Therefore, it is crucial to prevent the aggregation of MXene. Despite the discovery of various MXenes, Ti_3C_2 is the most extensively studied host material for LMAs. However, research on the MXene-based hosts for LMA is still in its early stages compared to other carbon-based nanomaterials.

3.1.2　MXene-based hybrids

As mentioned above, MXene could be served as an ideal host for LMA due to its exceptional metallic conductivity, high ion diffusion coefficient, and multifunctional surface groups. However, similar to other ultrathin 2D nanomaterials, MXene nanosheets could be easily agglomerated and restacked during the cycling process[76–78]. Therefore, the multifunctional surface groups are limited to be exposed, which eventually affects the morphology of Li on MXene. To overcome this challenge, lithiophilic seeds have been introduced to enhance the lithiophilicity of MXene, which helps regulate the burgeoning and nucleation of Li on the host material. The morphology of Li deposition on MXene could be further regulated by the synergistic effect of multifunctional surface groups on MXene with the introduced lithiophilic seeds. Besides, the introduction of carbon nanomaterials could effectively prevent the agglomeration and sustain the structural integrity of MXene nanosheets. Therefore, the incorporation of lithiophilic seeds and carbon nanomaterials could enable a stable and high-performance battery system based on MXene-hosted LMAs.

(1) MXene/0D hybrids

Metal nanoparticles act as lithiophilic nuclear agents uniformly deposited on layered MXene paper to ensure homogeneous lithium deposition and regulate the lithium dendrite's growth pathways and directions. Such as, Au could be dissolved into Li and then form a Li_xAu alloy phase, which could effectively minimize Li nucleation barriers when used as a host material for LMA[79–80]. Feng's group[81] designed a flexible MXene@Au *via* ion sputtering (Fig. 4a-e). The TEM image of MXene@Au indicated that the Au nanoparticles were confined on the thin, slightly crumple and self-supporting MXene nanosheets. As a result, this flexible anode showed significantly enhanced reversible capacity with high capacity retention of 98.47% even after 200 cycles.

In addition, Zn has the potential to be the lithiophilic nuclear agent to produce dendrites-free lithium anodes. Yang and co-workers made single zinc atoms

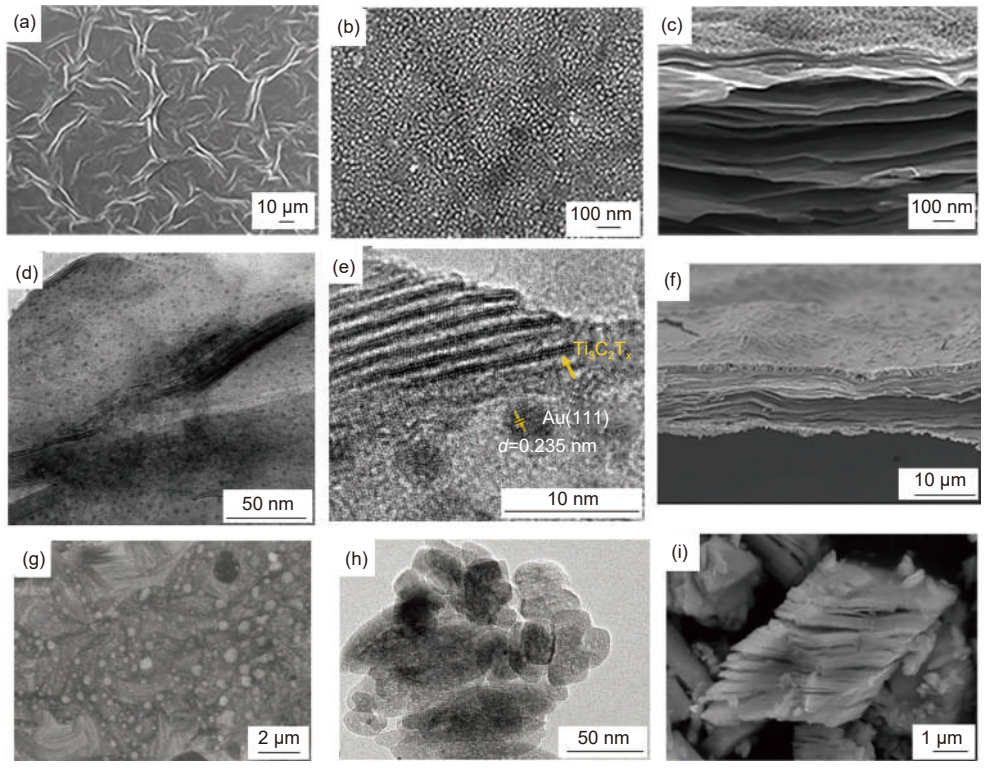

Fig. 4　(a) The Top view SEM images of MXene paper[81]; (b) The Top view SEM images of MXene@Au paper[81]; (c) Cross-sectional SEM image of MXene@Au paper[81]; (d) TEM image of $Ti_3C_2T_x$@Au paper[81]; (e) HRTEM image of $Ti_3C_2T_x$@Au paper[81]; (f) Cross-sectional SEM image a of $Ti_3C_2T_x$ MXene@Zn paper[83]; (g) Top view SEM images of MXene@RP paper[85]; (h) TEM images of MXene@RP paper[85]; (i) SEM image of NS-Nb_2C[86]. Reprinted with permission

fixed on MXene layers (Zn-MXene) as the host for lithium metal anodes[82]. The Zn-MXene-Li anode exhibited a stable and extended cycling life of 1 200 h at 1.0 mAh cm^{-2}, surpassing the cycling lives of MXene-Li (930 h) and Cu-Li (600 h) anodes. The Zn-MXene films and their hybrid lithium anodes possessed an advantage of facile manufacturing through the utilization of established rolling-to-rolling and spray coating technologies, thereby resulting in a significant reduction in costs. This, in turn, contributes to developing commercial lithium batteries. At the same time, Tian and his co-workers designed a freestanding $Ti_3C_2T_x$ MXene@Zn paper as the lithium metal anode host to address the challenges of dendrites growth (Fig. 4f)[83]. Over 600 cycles at 1 mAh cm^{-2} area capacity and 1 mA cm^{-2} current density, the modified anode displayed an average Coulombic efficiency of 97.69%, because of the outstanding mechanical flexibility, high electrical conductivity and lithiophilicity of the MXene@Zn paper. Moreover, ZnO was utilized by Li's group to modify the MXene-based host of lithium metal batteries due to its strong lithiophilic properties[84].

Apart from the metal nanoparticles, nonmetal element could also be used as lithiophilic seeds. Recently, a flexible paper composed of MXene@iodine-doped red phosphorus (MXene@RP) was designed by Na and Huang[85] through a straightforward method of vapor condensation reduction. The distribution of red phosphorus nanoparticles doped with iodine was uniform across both the surface and interlayer of the MXene matrix. During the vapor condensation process, the integrity of the MXene paper was well preserved at the same time (Fig. 4g-h). The anchorage of iodine-doped red phosphorus onto MXene was identified as a viable approach to prevent dendrite formation during lithium deposition. This was attributed to the improved conductivity of red phosphorus resulting from iodine doping, which in turn enhanced the kinetics of charge transfer. Hierarchical architectures were designed to enhance the ability of electroactive materials against volume fluctuations, while also facilitate ion diffusion pathways for lithium uptake. The utilization of a composite anode expands the applications of MXene and offers direction for developing the lithium hosts free of dendrites.

Except for the typical Ti_3C_2-MXene, nitrogen and sulfur co-doped Nb_2C MXene (NS-Nb_2C) anode has been synthesized by Zhang and Chen et al[86]. The obvious laminated structure of NS-Nb_2C can be seen in Fig. 4i. N and S doping sites could not only uniform Li deposition but enhance the electroconductivity of Nb_2C. The introduced heteroatoms could serve as extrinsic defects and lithiophilic active sites, open up the interlayer spacing and improve the conductivity of Nb_2C to suppress the dendrite growth. As such, the voltage-time curve of NS-Nb_2C demonstrated a notable degree of long-term stability with minimal fluctuation. Additionally, the resistance values of NS-Nb_2C were significantly lower than those of Nb_2C after undergoing 50 cycles. The NS-Nb_2C MXene has the potential to stimulate novel ideas for advanced LMAs.

The incorporation of lithiophilic zero-dimensional (0D) nanoparticles or nanodots into the MXene framework could facilitate the nucleation and growth of lithium, resulting in a homogeneous deposition of the element. In the process of Li plating, the preferential Li nucleation occurs around lithiophilic seeds. Uniform deposition of Li metal could be facilitated by the confinement of Li nucleation and growth inside the MXene matrix, which effectively suppresses the formation of "hot spots" and reduces favourable sites for dendrite growth. In additive to the examples listed above, other 0D materials, such as liquid metal[87], Ag[88], TiO_2[89], Sn[90–91] etc, have also been introduced into MXene as lithiophilic seeds for homogeneous Li deposition.

(2) MXene/1D hybrids

Several one-dimensional (1D) nanomaterials have been documented to be combined with MXene nanosheets to act as hosts for layered metal alloys (LMAs). The integration of 1D nanomaterials has been shown to improve mechanical properties and hinder the aggregation of MXene nanosheets[92]. As a typical example, the construction of a lithium host

with a lamellar structure that incorporates carbon nanotubes (CNTs), MXene nanosheets, and SnO_2 nanoparticles has been reported by Yan's research group *via* a simple step-by-step vacuum filtration method (Fig. 5a-b)[93]. The obtained multilayer stacked structure composite anode community of enough porosity, large surface area and high conductivity, showed the Coulombic efficiencies stabilized at 96%-98% at a high deposition capacities of 4 mAh cm^{-2} and delivered only 4.6% volume expansion during the high-capacity loading of 8 mAh cm^{-2}. Consequently, the designed lamellar structure was demonstrated as an efficient approach to buffer the volume variation. Furthermore, Wang[94] and his co-workers reported a particular topological structure by mixing cellulose nanofiber (CNF) with $Ti_3C_2T_x$ MXene as Li host (Fig. 5c-d). Such topological architecture is often prepared by vacuum filtration and rotational evaporation process. The utilization of interlocked topological microstructure, aided by CNF, facilitated the formation of micro-

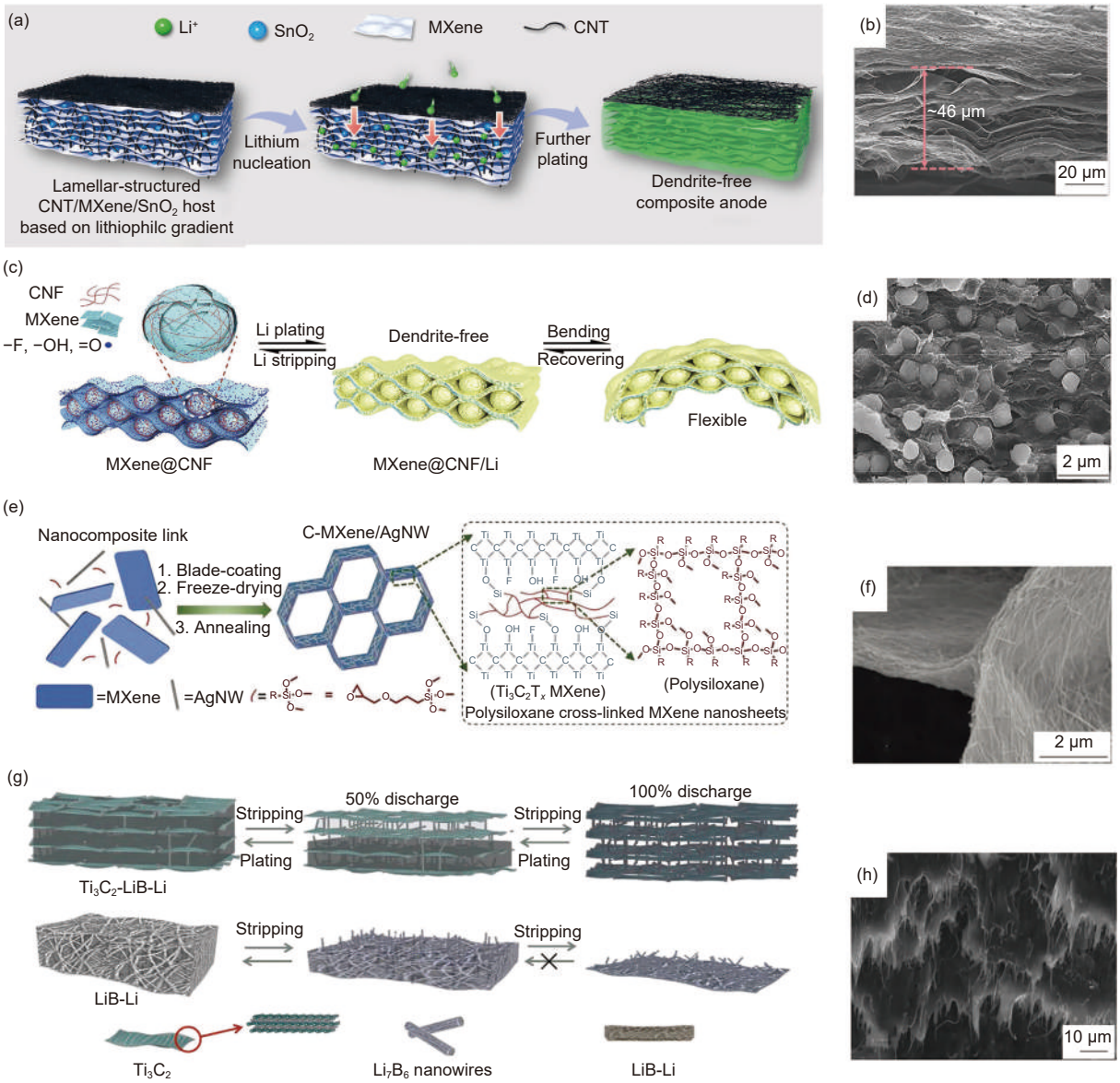

Fig. 5　(a) Schematic illustration of Li deposition in the lamellar-structured CNT/MXene/SnO_2 composite host based on lithiophilic gradient[93]; (b) Cross-sectional SEM image of the CNT/MXene/SnO_2 host[93]; (c) Schematic illustration of lithium plating on MXene@CNF film[94]; (d) Magnified SEM image of MXene@CNF film[94]; (e) Schematic illustration of the C-MXene/AgNW scaffold fabrication[95]; (f) Magnified SEM image showing a joint of the $C_{0.5}$-MXene/AgNW scaffold[95]; (g) The schematic diagram for the Li stripping-plating process of Ti_3C_2-LiB-Li hybrid and LiB-Li[96]; (h) The corresponding cross-section image of the Ti_3C_2-LiB-Li[96]. Reprinted with permission

spheres between MXene nanosheets through intermolecular hydrogen bonding. This significantly contributed towards augmenting the mechanical strength and flexibility of the MXene@CNF film. The Li metal anodes demonstrated remarkable long-term stability, as evidenced by a flat polarization voltage of 47 mV at 0.5 mA cm^{-2} for a duration exceeding 1 300 h without any indication of short-circuiting.

Not limited to CNFs, a conductive and lithiophilic scaffold was constructed by Liang's group[95] using polysiloxane and silver nanowire (AgNW). The former by cross-linking the MXene nanosheets *via* hydrolysis, polycondensation, and silylation reactions significantly enhanced the mechanical stability of the MXene-based scaffold. The later further improved the electrical conductivity and lithiophilicity of the MXene-based scaffold (Fig. 5e). The SEM images depicted the hierarchical structure of the $C_{0.5}$-MXene/AgNW scaffold, showcasing an average macropore size of approximately 10 μm and a mass density of roughly 0.154 8 g cm^{-3} (Fig. 5f). Mechanical strength and resilience were improved in the covalently cross-linked MXene host compared to the MXene scaffold. The utilization of cushioning mechanisms was beneficial in mitigating the significant internal stress fluctuations that arise from the rapid and deep plating-stripping of lithium. This approach also promoted the preservation of the integrated frame structure throughout the extended charging cycle. The lithium composite anode offered remarkable cyclic stability for lithium plating and stripping, resulting in an exceptional lifespan of 3 000 h. This stability was achieved even at an ultrahigh current density of 20 mA cm^{-2} and an areal capacity of 10 mAh cm^{-2}.

Furthermore, Zhao employed a technique of iteratively rolling and folding MXene-Ti_3C_2 nanosheets in conjunction with vertically aligned lithium-boron nanofibers (LiB) to produce a lithium hybrid with a multistorey corridor structure (Fig. 5g-h)[96]. The implementation of conductive Ti_3C_2 layers had the potential to impede the vertical expansion of lithium dendrites, while simultaneously enhanced the electrical conductivity of the mixed anode. This, in turn, could lead to a decrease in the local current density and uniform electric field. The lithophilicity Li_7B_6 nanofibers could be used as pillars between the Ti_3C_2 layers to prevent the multilayered corridor structure from collapsing and act as nucleating sites to induce the homogeneous deposition of lithium. The hybrid lithium anode was capable of functioning in exceeding settings, with a rate of 20 mA cm^{-2} and an area capacity of 10 mAh cm^{-2}.

(3) MXene/2D hybrids

Graphene oxide (GO) with good gelation ability is always used in assembing 3D structure from low-dimensional nanomaterials[97]. In 2018, Luo and his co-workers explored the MXene aerogel as a scaffold for Li metal anodes for the first time to improve the mechanical stability of traditional MXene nanosheets[98]. The plating/stripping process of Li in the MXene scaffold is depicted in Fig. 6a. The as-prepared framework inherited the porous structure and functional groups of the rGO aerogel (Fig. 6b). The utilization of MXene aerogel was observed to enhance the charging/discharging efficiency of LMA in the presence of high current densities.

In addition to 3D MXene aerogel anode, another important type of lithiophilic and flexible 3D porous anode $Ti_3C_2T_x$-rGO films was reported by Cao and his co-workers (Fig. 6c-d)[99]. The compact $Ti_3C_2T_x$-GO film was first fabricated by vacuum filtrating a certain amount of $Ti_3C_2T_x$ and GO solution, then contacting this membrane with molten Li by a spark reaction. Attributed to this innovative method, molten metal could be filled and sealed into the films, the composite film matrix along with expanding spacing and porosity performs excellent mechanical stability and flexibility. Thus, nucleation of molten Li was uniformed. Dendrites could be segregated and enclosed in separate interlayer cells and the MXene as well during the constant and repeating stripping/plating process. Consequently, the composite anode exhibited a remarkable specific capacity of 3 086 mAh g^{-1} and the cycling time up to 1 000 h at 2 C. The full cell of $LiFePO_4$ || Li-$Ti_3C_2T_x$-rGO exhibited superior capacity maintenance at 96.6% in comparison to the un-

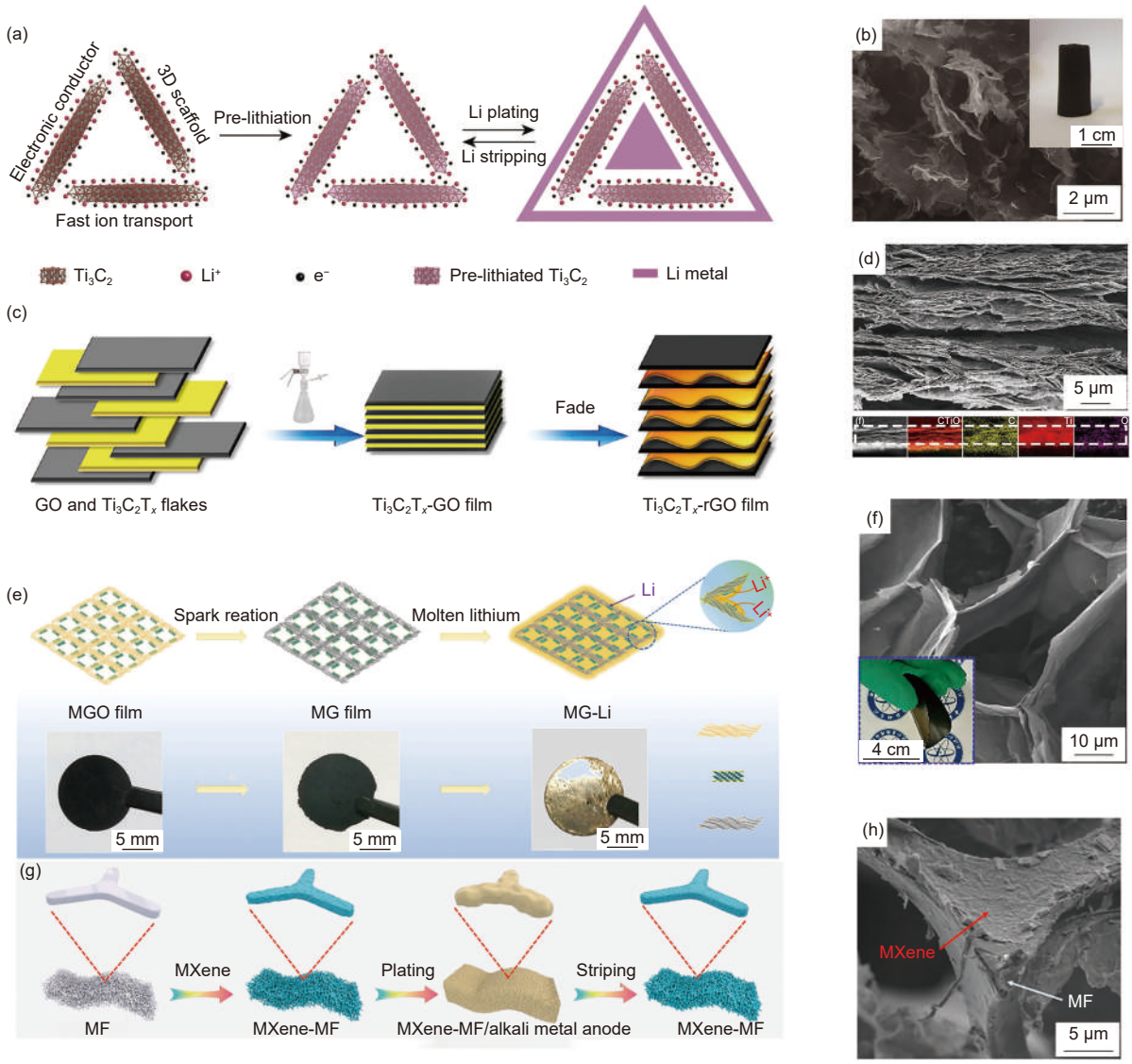

Fig. 6　(a) The Ti_3C_2 MXene aerogel scaffolds for Li metal anodes[98]; (b) SEM image of the MXene/rGO aerogel. Inset: a photograph of the aerogel[98]; (c) Schematic diagram of Li-$Ti_3C_2T_x$-rGO preparation[99]; (d) SEM cross-section images of $Ti_3C_2T_x$-rGO[99]; (e) Schematic illustration of the fabrication process of the 3D MG-Li anode and corresponding photographs of the MGO film, MG film, and MG-Li anode[100]; (f) SEM image of the MG film. Inset is a photograph of the bent MG film[100]; (g) Schematic illustration of the fabrication process of the 3D MXene-MF for the alkali-metal anode[101]; (h) SEM image of MXene-MF[101]. Reprinted with permission

modified Li cells (90.1%).

The large gap between theoretical and practical electrochemical properties for the lithium metal battery system should be filled by adopting a series of design architectures towards withstand large current density and high Li loading. For this, Wu's[100] group proposed a lightweight, porous, freestanding, mechanically stable MXene/graphene (MG) framework as a host for LMAs (Fig. 6e-f). The 3D MG anode had a rich interconnected pore structure with a high surface area (259 $m^2\ g^{-1}$) and capacity as high as 3 560 mAh g^{-1} coupled with Coulombic efficiencies (>99%) without Li dendrites. The composite materials exhibited exceptional cycling stability for 120 h at 20 mA cm^{-2} without obvious voltage decay and short-circuit. Soon afterwards, they designed a 3D flexible and conductive $Ti_3C_2T_x$ MXene-melamine foam (MXene-MF) as a host for the LMA (Fig. 6g-h)[101]. This 3D composite anode showed both high electrochemical performance and high durability.

Apart from the carbon-based materials, covalent organic frameworks (COFs), a category of porous crystalline materials that consist of recurring organic building units that are interconnected by covalent

bonds, have received great attention for application in modified lithium metal anode, since they have the properties of durable stability, big porosity, and low density, sufficient specific surface area. For example, Lai[102] and his co-workers covalently assembled COFs on MXene nanosheets to enable fast-charging lithium hosts by amination and *in-situ* deposition. After embellishing with the ultrathin 2D COF-LZU1, the MXene@COF showed high crystallinity, hierarchical porosity, and conductive frameworks, greatly improved lithium storage and charge transport, resulting in the long-term cyclability of 106 mAh g^{-1} after 150 cycles.

Based on the above discussion, it could be inferred that the incorporation of lithiophilic moieties, such as Au and Zn, *via* surface/interface modification, represented a highly efficacious approach to enhancing the affinity towards LMAs. As the hosts for LMAs, a combination of MXene and 1D nanomaterials (CNF, CNT and AgNW) showed extraordinarily long-term reversible Li plating-stripping at ultrahigh current densities with ultrahigh areal capacities while maintaining the structural integrity of scaffold across thousands of cycles. Besides, researchers succeed to explore the MXene-based aerogel as a high-performance scaffold for LMAs that delivered a high specific capacity. The fabrication of MXene/2D hybrid nanomaterials through introducing other 2D nanomaterials improved the lithiophilicity or mechanical properties. Meanwhile, it could provide enlarged interlayer spaces or necessary porous channels for Li plating/infusion. Constructing MXene-based hybrid nanoarchitectures has become a promising strategy to develop advanced stable and dendrite-free LMAs. The applications of MXene for LMAs and their corresponding electrochemical performances have been summarized in Table 1.

3.1.3 MXene derivatives

In addition to the development of MXene-based hybrid nanoarchitectures, MXene-derived hybrid nanoarchitectures have been developed as Li hosts to facilitate the Li infusion and uniform deposition. Recently, Peng's group[103] prepared a new MXene derivative containing pure rutile TiO_2 and N-doped carbon. Firstly, heated the precursor MXene under a mixing gas of NH_3: Ar (1 ∶ 9) at 800 °C and then formed the TiO_2/N-doped C hybrid. Secondly, injected molten Li into it. After Li infusion, 3D layered TiO_2/N-doped C and TiO_2/C samples were achieved. Thus, the Li cells with the $LiTiO_2$-Li_3N-C electrode delivered an extremely long cycle life of 2 000 h at 1 mA cm^{-2} and an overpotential of only 30 mV.

Table 1 Summary of the MXene-based nanomaterials for Li-metal anodes

Electrodes	Current density/(mA cm^{-2})	Capacity/(mAh cm^{-2})	Electrolyte	Overpotential/mV	Cycle life/h	Ref.
Ti_3C_2 MXene (graphene, BN)	1 mA cm^{-2}	1 mAh cm^{-2}	1 M $LiPF_6$ in EC/DMC (1 ∶ 1, *v*/*v*)	32 mV	400 h	[66]
ILC-Li	3 mA cm^{-2}	3 mAh cm^{-2}	1 M $LiPF_6$ in EC/EMC (3 ∶ 7, weight/weight) with 2wt% VC	15-20 mV	2250 h	[69]
3DP-MXene arrays	1 mA cm^{-2}	1 mAh cm^{-2}	1 M LiTFSI in DOL/DME (1 ∶ 1, *v*/*v*) with 1wt% $LiNO_3$	10 mV	1200 h	[75]
MXene@Au	1 mA cm^{-2}	1 mAh cm^{-2}	1 M LiTFSI in DOL/DME (1 ∶ 1, *v*/*v*) with 2wt% $LiNO_3$	/	650 h	[81]
Zn-MXene	1 mA cm^{-2}	1 mAh cm^{-2}	1 M LiTFSI in DOL/DME (1 ∶ 1, *v*/*v*).	16 mV	1200 h	[82]
MXene/ZnO	1 mA cm^{-2}	1 mAh cm^{-2}	2 M LiTFSI in DME with 1wt% FEC	37±6 mV	250 h	[84]
CNT/MXene/SnO_2	40 mA cm^{-2}	1 mAh cm^{-2}	1 M $LiPF_6$ in EC/EMC (1 ∶ 1, *v*/*v*) with 15wt% FEC	85 mV	500 cycles	[93]
MXene@CNF	0.5 mA cm^{-2}	1 mAh cm^{-2}	1 M LiTFSI in DOL/DME (1 ∶ 1, *v*/*v*) with 1wt% $LiNO_3$	47 mV	1300 h	[94]
Ti_3C_2-LiB-Li	1 mA cm^{-2}	1 mAh cm^{-2}	1 M LiTFSI in DOL/DME (1 ∶ 1, *v*/*v*) with 1wt% $LiNO_3$	/	1000 h	[96]
$Ti_3C_2T_x$-rGO	1 mA cm^{-2}	1 mAh cm^{-2}	1M $LiPF_6$ in EC/DMC/EMC (1 ∶ 1:1, *v*/*v*/v) with 5.0% FEC	36 mV	1400 h	[99]
3D MG	5 mA cm^{-2}	1 mAh cm^{-2}	1 M LiTFSI in DOL/DME (1 ∶ 1, *v*/*v*) with 1wt% $LiNO_3$	25 mV	400 h	[100]
MXene-MF	5 mA cm^{-2}	5 mAh cm^{-2}	1 M LiTFSI in DOL/DME (1 ∶ 1, *v*/*v*) with 1wt% $LiNO_3$.	13 mV	700 h	[101]

Note: M: mol L^{-1}

3.2 Constructing MXene-based artificial SEI films

A desirable SEI ought to have a proper thickness, high ionic conductivity, strong mechanical performance, low interfacial resistance, extraordinary stability and steady chemistry during long-term cycles and deep plating-stripping for safe and efficient LMBs. Regretfully, the traditional SEI does not present the above characteristics. There are a lot of strategies that have been investigated to create an artificial and resilient layer to prevent uncontrolled processes during SEI formation. For example, Gong's group[104] synthesized 2D/2D $Ti_3C_2Tx/g\text{-}C_3N_4$ nanosheets heterojunction with *in-situ* grown $g\text{-}C_3N_4$ by pyrolysis process and used it as artificial SEI film to inhibit the growth of Li dendrites (Fig. 7a). The synthesis method not only built stable connection points between $Ti_3C_2T_x$ and $g\text{-}C_3N_4$, but also avoided the agglomeration of $Ti_3C_2T_x$ nanosheets. The as-prepared $Ti_3C_2Tx/g\text{-}C_3N_4$ hybrid showed a crinkled sheet-like morphology with a thickness of 3.2 nm (Fig. 7b). The obtained composite electrode enabled the conformal Li deposition in the plating process, efficiently increasing the rapid transport of Li-ion. In addition. The primary constituent in the inner layer of SEI was Li_3N and LiF deriving from Li interaction with N element of $g\text{-}C_3N_4$ and -F surface termination groups of $Ti_3C_2T_x$ respectively. The $Ti_3C_2T_x/g\text{-}C_3N_4$ electrode showed a reduced nucleation overpotential of 14.0 mV , which was significantly less than the electrode material $Ti_3C_2T_x$ (Fig. 7c). The full-cell when coupled with the cathode of NCM811 (with an areal capacity of 1.2 mAh cm^{-2}), exhibited an initial specific capacity of 167.2 mAh g^{-1} at 0.3 C. This capacity remained stable over 110 cycles with capacity retention of 81.2%.

Liu et al.[105] fabricated a synthetic polymer/2D $Ti_3C_2T_x$ (MXene) SEI on a lithium metal substrate. Fig. 7d depicts the procedure for producing a lithium metal anode with an artificial solid electrolyte interphase (SEI). Initially, the MXene powders were amalgamated with 1,3-dioxolane (DOL) and 1,2-dimethoxyethane (DME). Subsequently, the suspension was supplemented with particles of Li bistrifluoromethanesulfonimide (LiTFSI) and lithium hexafluorophosphate ($LiPF_6$). Finally, the homogeneous distribution of monomers was expeditiously applied to the lithium foil. The polymer layer offered good interface contact and excellent adaptability to reduce interface

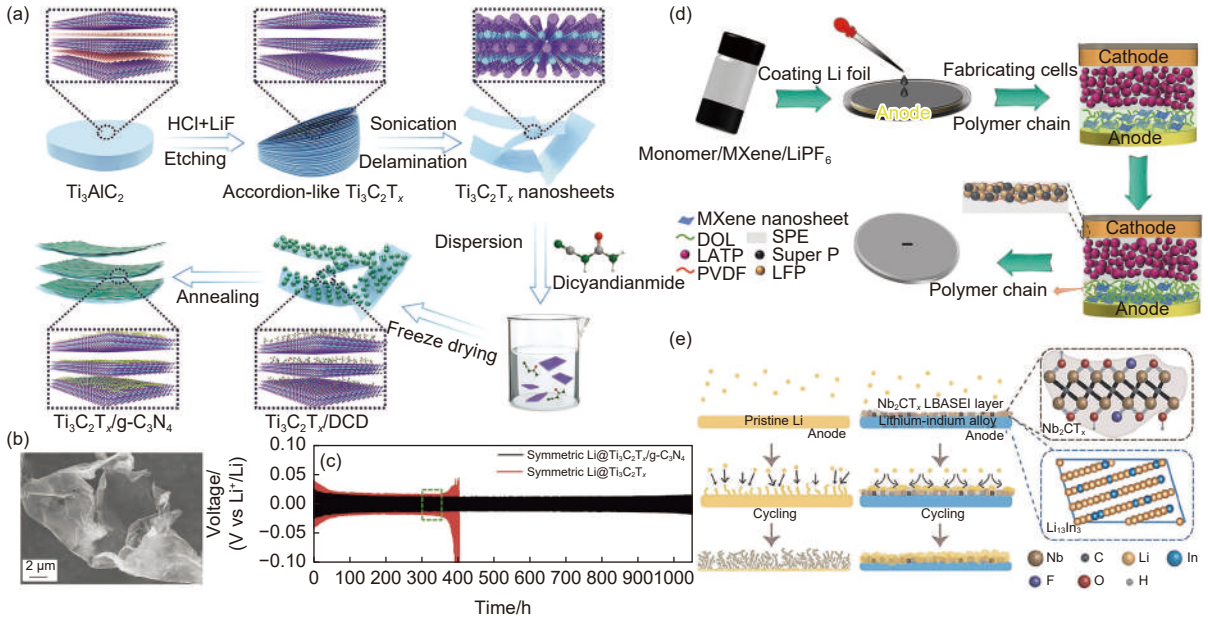

Fig. 7　(a) Schematic illustration of the fabrication process of $Ti_3C_2T_x/g\text{-}C_3N_4$ hybrid[104]; (b) SEM image of $Ti_3C_2T_x/g\text{-}C_3N_4$[104]; (c) Voltage-time profiles of Li plating/stripping in different symmetric cells with the capacity of 0.5 mAh cm^{-2} at 0.5 mA cm^{-2} and Detailed voltage profiles for selective cycles in panel[104]; (d) Schematic diagram of the in-situ generation process of MA-SEI in the Li metal anode interface[105]; (e) Schematic illustration for the Li deposition and migration processes occurring at the Nb_2CT_X Li-In alloy anode[106]. Reprinted with permission

resistance. The 2D MXene with a low Li nucleation energy barrier was advanced to uniformly deposited Li and restrain the side reaction. The Li/SSE/Li configuration exhibited a consistent polarization voltage of around 50 mV when operating at a capacity of 0.5 mAh cm^{-2} and kept this exceeding performance for 1 000 h.

Lithium alloy is a promising candidate for LMAs. In 2022, Won[106] used a Li-In alloy as an anode material and combined it with Nb_2CT_x MXene as an artificial solid-electrolyte interphase, which was referred to as Nb_2CT_x Li-In. Fig. 7e presents a schematic representation of the Li deposition and migration mechanisms observed on both the bare Li anode and the Nb_2CT_x Li-In alloy anode. The former demonstrated a notable affinity for Li and facilitates the appropriate migration of Li ions, thereby promoting the stable electrodeposition of Li. Moreover, pouch cells consisted of Nb_2CT_x Li-In alloy anodes and NCM811 cathodes delivered an energy density of 272 Wh kg^{-1} and 500 Wh L^{-1}. The Nb_2CT_x Li-In alloy anode could proficiently alleviate the regional expansion caused by Li dendrites and inhibiting side reactions.

The separator is crucial in rechargeable batteries as it prevents an internal short circuit by separating the cathode and anode. The development of effective separators for high-performance lithium metal batteries is a crucial driving force for the prevention of lithium dendrite growth[107–112]. For example, Han[113] and his co-workers designed an engineered interphases separator modified by two-dimensional layered $Ti_3C_2T_x$ and the solid-state electrolyte $Li_{1.3}Al_{0.3}Ge_{1.7}(PO_4)_3$ (LAGP) synthesized via solid-state reaction method for homogenization Li plating. The homogeneous transmission of lithium ions and electrons was facilitated by the extensively blended conductive properties of LAGP/MXene. The morphological changes of Li metal in full cells was revealed that the Li metal anodes experienced a volume expansion of 257% when paired with PP separators. This expansion was approximately nine times greater than that observed when PP/LAGP+MXene separators were used, which exhibited a volume expansion of only 28%. In addition, the in situ formed Ge, Li_3PO_4, and LiF interphases, which were derived from the reduction of LAGP, contributed to the stabilization of SEI. The symmetric cells utilizing PP/LAGP+MXene separators exhibited a consistent voltage for Li plating/stripping for a duration of more than 700 h when subjected to a current density of 1 mA cm^{-2} within an area capacity of 1 mAh cm^{-2}. The utilization of the modified separator in the full-cell configuration led to a notable improvement in its cycling stability. The analysis of the action mechanism of the material on the separator provided a new insight for prolonging the life of lithium metal anodes.

3.3 MXene-based electrolyte additives

To overcome the safety problems caused by the flammability of the organic electrolyte in the case of overcharging or short-circuiting, all-solid-state lithium metal batteries (LMBs) have been proposed by the research community. Different species of solid electrolytes could be classified into 4 sections, including polymer solid electrolytes, inorganic solid electrolytes, solid polymer electrolytes, and composite solid electrolytes[114]. Nanocomposite polymer electrolytes (CPEs) exhibited potential as viable materials for all-solid-state lithium metal batteries (LMBs) owing to their improved ionic conductivities, outstanding viscoelasticity, fast film formation, lightweight and stability to the lithium anode[115]. Christopher Y Li and his group studied the critical role of MXenes as an electrolyte addictive on the electrochemical performance of all-solid-state lithium metal batteries at room temperature. To create MXene-based CPEs (MCPEs), they employed a green, facile aqueous solution blending process to uniformly spread small amounts of $Ti_3C_2T_x$ within a poly (ethylene oxide)/LiTFSI complex (PEO_{20}-LiTFSI). Their research proved that MXenes as an electrolyte additive could inhibit polymer crystallization, improve the peristalsis of polymer segments, and increase the concentration of carriers. Meanwhile, MXenes nanosheets with negative charges could attract lithium cations to improved transference number and ionic conductivities which are 6 orders of magnitude higher than the CPEs. Meanwhile, it was encouraging to see that the high-rate partial state of charge capacity of the MCPEs cell under 1 C rate was 92 mAh g^{-1}. The temperature-de-

pendent conductivity data was tested using the modified Vogel-Tammann-Fulcher (VTF) equation, the results indicated that the CPE with 3.6% (mass fraction) MXene showed a higher ionic conductivity at room temperature (2.2×10^{-5} S m^{-1} at 28 °C)[116] than its counterparts.

4 Summary and outlook

Lithium metal battery is a type of promising energy storage device due to the high energy density. But inherent issues including uncontrollable dendrites and low Coulombic efficiency (CE) impede their commercialization. MXene, as an emerging 2D material, has demonstrated significant potential in addressing the inherent issues associated with metal anodes. This is due to their exceptional mechanical properties, abundant surface functional groups, high electronic and ionic conductivity. In conclusion, we summarized the working principle, construction, and a few important advances of 2D MXene utilized for stable and dendrites-free Li metal anodes in this review, including designing MXene-based LMA hosts, constructing MXene-based artificial SEI films, and modifying MXene-based electrolyte additives. The surface/interface modification involving lithiophilic groups (e.g. Au, Zn, N and S) presented as a promising approach to enhance the affinity for Li metal anode. This strategy could facilitate the creation of additional nucleation sites, promote uniform nucleation, and significantly enhance the stability of LMAs. In addition, designing nanosheet arrays of MXene as lithium metal host electrodes significantly improves the cycling stability and rate capability of LMAs.

The analysis shows that MXene, an emerging 2D material, has been extensively used for stabilizing the LMAs. By modifying the LMAs with 2D MXene, the issues of dendrites growth, large volume changes, and an unstable SEI could be effectively addressed. Despite the improvements in electrochemical performance, commercializing LMAs still face several challenges. To further enhance their praticalibility, future work should prioritize the following aspects:

(1) Enhance the efficiency and decrease the cost of MAX phases and MXenes during the large-scale synthesis, which requires more efforts from both fundamental studies and scale-up engineering techniques.

(2) Combine theoretical studies and experimental research in depth to study and apply various kinds of MXenes besides the Ti-based MXenes.

(3) Although MXene works efficiently on Li metal anodes in preventing dendrite growth and volume changes, more research is required to develop MXene-based skeletons/SEI layers/additives for Na-metal, K-metal, and Zn-metal anodes in the future.

(4) Considering the unclear inhibition mechanism of lithium dendrites with MXene-based nanomaterials, advanced characterization techniques, such as cryogenic electron microscopy (cryo-EM), Auger electron spectroscopy (AES), and nuclear magnetic resonance (NMR), etc, could be applied to understand the inherent link among lithium metal nucleation, dendrite growth, defects, crystal morphology, and MXene-based skeletons/SEI layers/additives.

Acknowledgements

The authors acknowledge financial support by the National Natural Science Foundation of China (52225208, U21A20174, 51972285 and 52202314).

References

[1] Tarascon J M, Armand M. Building better batteries[J]. Nature, 2008, 451(7179): 652-657.

[2] Liu Y M, Zhang Y J, Cheng K, et al. Inside cover: Selective electrochemical reduction of carbon dioxide to ethanol on a boron- and nitrogen-co-doped nanodiamond[J]. Angewandte Chemie, 2017, 56(49): 15474-15474.

[3] Etacheri V, Marom R, Elazari R, et al. Challenges in the development of advanced Li-ion batteries: A review[J]. Energy & Environmental Science, 2011, 4(9): 3243-3262.

[4] Lin D C, Liu Y Y, Cui Y. Reviving the lithium metal anode for high-energy batteries[J]. Nature Nanotechnology, 2017, 12(3): 194-206.

[5] Xu W, Wang J L, Ding F, et al. Lithium metal anodes for rechargeable batteries[J]. Energy & Environmental Science, 2014, 7(2): 513-537.

[6] Tarascon J M, Armand M. Issues and challenges facing rechargeable lithium batteries[J]. Nature, 2001, 414(6861): 359-367.

[7] Li N W, Yin Y X, Yang C P, et al. An artificial solid electrolyte interphase layer for stable lithium metal anodes[J]. Advanced Materials, 2016, 28(9): 1853-1858.

[8] Wang L P, Wang Q J, Jia W S, et al. Li metal coated with

amorphous Li_3PO_4 via magnetron sputtering for stable and long-cycle life lithium metal batteries[J]. Journal of Power Sources, 2017, 342: 175-182.

[9] Baloch M, Shanmukaraj D, Bondarchuk O, et al. Variations on Li_3N protective coating using ex-situ and in-situ techniques for Li degree in sulphur batteries[J]. Energy Storage Materials, 2017, 9: 141-149.

[10] Yan C, Yao Y X, Chen X, et al. Lithium nitrate solvation chemistry in carbonate electrolyte sustains high-voltage lithium metal batteries[J]. Angewandte Chemie, 2018, 57(43): 14292-14292.

[11] Patra J, Huang H T, Xue W J, et al. Moderately concentrated electrolyte improves solid-electrolyte interphase and sodium storage performance of hard carbon[J]. Energy Storage Materials, 2019, 16: 146-154.

[12] Wang M Q, Peng Z, Luo W W, et al. Tailoring lithium deposition via an SEI-functionalized membrane derived from LiF decorated layered carbon structure[J]. Advanced Energy Materials, 2019, 9(12): 1802912.

[13] Liu Y J, Tao X Y, Wang Y, et al. Self-assembled monolayers direct a LiF-rich interphase toward long-life lithium metal batteries[J]. Science, 2022, 375(6582): 739-745.

[14] Li Y T, Xu B Y, Xu H H, et al. Hybrid polymer/garnet electrolyte with a small interfacial resistance for lithium-ion batteries[J]. Angewandte Chemie, 2017, 129(3): 771-774.

[15] Sheng O W, Jin C B, Ju Z J, et al. Stabilizing Li_4SnS_4 electrolyte from interface to bulk phase with a gradient lithium iodide/polymer layer in lithium metal batteries[J]. Nano Letters, 2022, 22(20): 8346-8354.

[16] Wan J Y, Xie J, Kong X, et al. Ultrathin, flexible, solid polymer composite electrolyte enabled with aligned nanoporous host for lithium batteries[J]. Nature Nanotechnology, 2019, 14(7): 705-711.

[17] Lin D C, Yuen P Y, Liu Y Y, et al. A silica-aerogel-reinforced composite polymer electrolyte with high ionic conductivity and high modulus[J]. Advanced Materials, 2018, 30(32): 1802661.

[18] Chi S S, Liu Y C, Zhao N, et al. Solid polymer electrolyte soft interface layer with 3D lithium anode for all-solid-state lithium batteries[J]. Energy Storage Materials, 2019, 17: 309-316.

[19] Sun C Z, Li Y P, Jin J, et al. ZnO nanoarray-modified nickel foam as a lithiophilic skeleton to regulate lithium deposition for lithium-metal batteries[J]. Journal of Materials Chemistry A, 2019, 7(13): 7752-7759.

[20] Deng W, Zhou X F, Fang Q, et al. Microscale lithium metal stored inside cellular graphene scaffold toward advanced metallic lithium anodes[J]. Advanced Energy Materials, 2018, 8(12): 1703152.

[21] Naguib M, Kurtoglu M, Presser V, et al. Two-dimensional nanocrystals: Two-dimensional nanocrystals produced by exfoliation of Ti_3AlC_2[J]. Advanced Materials, 2011, 23(37): 4207-4207.

[22] Luo J M, Zheng J H, Nai J W, et al. Atomic sulfur covalently engineered interlayers of Ti_3C_2 MXene for ultra-fast sodium-ion storage by enhanced pseudocapacitance[J]. Advanced Functional Materials, 2019, 29(10): 1808107.

[23] Naguib M, Mochalin V N, Barsoum M W, et al. 25th anniversary article: MXenes: A new family of two-dimensional materials[J]. Advanced Materials, 2014, 26(7): 992-1005.

[24] Sarycheva A, Gogotsi Y. Raman spectroscopy analysis of the structure and surface chemistry of $Ti_3C_2T_x$ MXene[J]. Chemistry of Materials, 2020, 32(8): 3480-3488.

[25] Urbankowski P, Anasori B, Makaryan T, et al. Synthesis of two-dimensional titanium nitride Ti_4N_3 (MXene)[J]. Nanoscale, 2016, 8(22): 11385-11391.

[26] Halim J, Kota S, Lukatskaya M R, et al. Synthesis and characterization of 2D molybdenum carbide (MXene)[J]. Advanced Functional Materials, 2016, 26(18): 3118-3127.

[27] Nan J X, Guo X, Xiao J, et al. Nanoengineering of 2D MXene-based materials for energy storage applications[J]. Small, 2021, 17(9): 1902085.

[28] Sun W, Shah S A, Chen Y, et al. Electrochemical etching of Ti_2AlC to Ti_2CT_x (MXene) in low-concentration hydrochloric acid solution[J]. Journal of Materials Chemistry A, 2017, 5(41): 21663-21668.

[29] Yang S, Zhang P P, Wang F X, et al. Fluoride-free synthesis of two-dimensional titanium carbide (MXene) using a binary aqueous system[J]. Angewandte Chemie, 2018, 57(47): 15491-15495.

[30] Ding R, Lyu Y, Wu Z, et al. Effective piezo-phototronic enhancement of flexible photodetectors based on 2D hybrid perovskite ferroelectric single-crystalline thin-films[J]. Advanced Materials, 2021, 33(32): 2170252.

[31] Li T F, Yao L L, Liu Q L, et al. Fluorine-free synthesis of high-purity $Ti_3C_2T_x$ (T=OH, O) via alkali treatment[J]. Angewandte Chemie, 2018, 57(21): 6115-6119.

[32] Natu V, Pai R, Sokol M, et al. 2D $Ti_3C_2T_z$ MXene synthesized by water-free etching of Ti_3AlC_2 in polar organic solvents[J]. Chem, 2020, 6(3): 616-630.

[33] Li Y B, Shao H, Lin Z F, et al. A general lewis acidic etching route for preparing MXenes with enhanced electrochemical performance in non-aqueous electrolyte[J]. Nature Materials, 2020, 19(8): 894-899.

[34] Xiao X, Yu H M, Jin H Y, et al. Salt-templated synthesis of 2D metallic mon and other nitrides[J]. ACS Nano, 2017, 11(2): 2180-2186.

[35] Mei J, Ayoko G A, Hu C, et al. Thermal reduction of sulfur-containing MAX phase for MXene production[J]. Chemical engineering journal, 2020, 395: 125111.

[36] Xu C, Wang L B, Liu Z B, et al. Large-area high-quality 2D ultrathin Mo_2C superconducting crystals[J]. Nature Materials, 2015, 14(11): 1135-1141.

[37] Luo J M, Matios E, Wang H, et al. Interfacial structure design of MXene-basednanomaterials for electrochemical energy storage and conversion[J]. InfoMat, 2020, 2(6): 1057-1076.

[38] Luo J M, Fang C, Jin C B, et al. Tunable pseudocapacitance storage of MXene by cation pillaring for high performance sodium-ion capacitors[J]. Journal of Materials Chemistry A, 2018, 6(17): 7794-7806.

[39] Cho K T, Ridgway P, Weber A Z, et al. Erratum: High

performance hydrogen/bromine redox flow battery for grid-scale energy storage[J]. Journal of the Electrochemical Society, 2013, 160(8): X9-X9.

[40] Albertus P, Girishkumar G, McCloskey B, et al. Identifying capacity limitations in the li/oxygen battery using experiments and modeling[J]. Journal of the Electrochemical Society, 2011, 158(3): A343-A351.

[41] Shen X, Liu H, Cheng X B, et al. Beyond lithium ion batteries: Higher energy density battery systems based on lithium metal anodes[J]. Energy Storage Materials, 2018, 12: 161-175.

[42] Zhang T, Zhang L, Hou Y L. MXenes: Synthesis strategies and lithium-sulfur battery applications[J]. eScience, 2022, 2(2): 164-182.

[43] Wang Q, Liu B, Shen Y, et al. Confronting the challenges in lithium anodes for lithium metal batteries[J]. Advanced Science, 2021, 8(17): 2101111.

[44] Howlett P C, MacFarlane D R, Hollenkamp A F. A sealed optical cell for the study of lithium-electrode| electrolyte interfaces[J]. Journal of Power Sources, 2003, 114(2): 277-284.

[45] Albertus P, Babinec S, Litzelman S, et al. Status and challenges in enabling the lithium metal electrode for high-energy and low-cost rechargeable batteries[J]. Nature Energy, 2018, 3(1): 16-21.

[46] Zhang X Y, Wang A X, Liu X J, et al. Dendrites in lithium metal anodes: Suppression, regulation, and elimination[J]. Accounts of Chemical Research, 2019, 52(11): 3223-3232.

[47] Chazalviel J N. Electrochemical aspects of the generation of ramified metallic electrodeposits[J]. Physical Review, 1990, 42(12): 7355-7367.

[48] Fleury V, Chazalviel J N, Rosso M, et al. The role of the anions in the growth speed of fractal electrodeposits[J]. Journal of Electroanalytical Chemistry and Interfacial Electrochemistry, 1990, 290(1): 249-255.

[49] Liang Y R, Xiao Y, Yan C, et al. A bifunctional ethylene-vinyl acetate copolymer protective layer for dendrites-free lithium metal anodes[J]. Journal of Energy Chemistry, 2020, 48: 203-207.

[50] Yamaki J, Tobishima S, Hayashi K, et al. A consideration of the morphology of electrochemically deposited lithium in an organic electrolyte[J]. Journal of Power Sources, 1998, 74(2): 219-227.

[51] Wang X, Zeng W, Hong L, et al. Stress-driven lithium dendrite growth mechanism and dendrite mitigation by electroplating on soft substrates[J]. Nature Energy, 2018, 3(3): 227-235.

[52] Peled E. The electrochemical-behavior of alkali and alkaline-earth metals in non-aqueous battery systems-the solid electrolyte interphase model[J]. Journal of the Electrochemical Society, 1979, 126(12): 2047-2051.

[53] Peled E, Menkin S. Review-SEI: Past, present and future[J]. Journal of the Electrochemical Society, 2017, 164(7): A1703-A1719.

[54] Thevenin J G, Muller R H. Impedance of lithium electrodes in a propylene carbonate electrolyte[J]. Journal of the Electrochemical Society, 1987, 134(2): 273-280.

[55] Verma P, Maire P, Novák P. A review of the features and analyses of the solid electrolyte interphase in Li-ion batteries[J]. Electrochimica Acta, 2010, 55(22): 6332-6341.

[56] Aurbach D, Chusid O. In situ FTIR spectroelectrochemical studies of surface films formed on Li and nonactive electrodes at low potentials in Li salt solutions containing CO_2[J]. Journal of the Electrochemical Society, 1993, 140(11): L155-L157.

[57] Odziemkowski M, Irish D E. An electrochemical study of the reactivity at the lithium electrolyte/bare lithium metal interface I. Purified electrolytes[J]. Journal of the Electrochemical Society, 1992, 139(11): 3063-3074.

[58] Kanamura K, Shiraishi S, Takehara Z. Electrochemical deposition of very smooth lithium using nonaqueous electrolytes containing HF[J]. Journal of the Electrochemical Society, 1996, 143(7): 2187-2197.

[59] Ghazi Z A, Sun Z, Sun C, et al. Key aspects of lithium metal anodes for lithium metal batteries[J]. Small, 2019, 15(32): 1900687.

[60] Shi P, Li T, Zhang R, et al. Lithiophilic LiC_6 layers on carbon hosts enabling stable li metal anode in working batteries[J]. Advanced Materials, 2019, 31(8): 1807131.

[61] Hu W, Zheng M, Xu B, et al. Design of hollow carbon-based materials derived from metal-organic frameworks for electrocatalysis and electrochemical energy storage[J]. Journal of Materials Chemistry A, 2021, 9(7): 388-3917.

[62] Zhu Z, Liu Y, Ju Z, et al. Synthesis of diverse green carbon nanomaterials through fully utilizing biomass carbon source assisted by KOH[J]. ACS Applied Materials & Interfaces, 2019, 11(27): 24205-24211.

[63] Chi S S, Liu Y, Song W L, et al. Prestoring lithium into stable 3D nickel foam host as dendrite-free lithium metal anode[J]. Advanced Functional Materials, 2017, 27(24): 1700348.

[64] Fan W, Li N W, Zhang X, et al. A dual-salt gel polymer electrolyte with 3D cross-linked polymer network for dendrite-free lithium metal batteries[J]. Advanced Science, 2018, 5(9): 1800559.

[65] Lucero N, Vilcarino D, Datta D, et al. The roles of MXenes in developing advanced lithium metal anodes[J]. Journal of Energy Chemistry, 2022, 69: 132-149.

[66] Li B, Zhang D, Liu Y, et al. Flexible Ti_3C_2 MXene-lithium film with lamellar structure for ultrastable metallic lithium anodes[J]. Nano Energy, 2017, 39: 654-661.

[67] Zhang D, Wang S, Li B, et al. Horizontal growth of lithium on parallelly aligned MXene layers towards dendrite-free metallic lithium anodes[J]. Advanced Materials, 2019, 31(33): 1901820.

[68] Gu J, Chen H, Shi Y, et al. Eliminating lightning-rod effect of lithium anodes via sine-wave analogous MXene layers[J]. Advanced Energy Materials, 2022, 12(36): 2201181.

[69] Chen X, Shang M, Niu J. Inter-layer-calated thin li metal electrode with improved battery capacity retention and dendrite suppression[J]. Nano Letters, 2020, 20(4): 2639-2646.

[70] Chen Q, Wei Y, Zhang X, et al. Vertically aligned MXene nanosheet arrays for high-rate lithium metal anodes[J]. Advanced Energy Materials, 2022, 12(18): 2200072.

[71] Cao Z, Zhu Q, Wang S, et al. Perpendicular MXene arrays with periodic interspaces toward dendrite-free lithium metal anodes with high-rate capabilities[J]. Advanced Functional Materials,

2020, 30(5): 1908075.

[72] Tian X, Jin J, Yuan S, et al. Emerging 3D-printed electrochemical energy storage devices: A critical review[J]. Advanced Energy Materials, 2017, 7(17): 1700127.

[73] Zhang C, McKeon L, Kremer M P, et al. Additive-free MXene inks and direct printing of micro-supercapacitors[J]. Nature Communications, 2019, 10(1): 1795-1795.

[74] Li K, Liang M, Wang H, et al. 3D MXene architectures for efficient energy storage and conversion[J]. Advanced Functional Materials, 2020, 30(47): 2000842.

[75] Shen K, Li B, Yang S. 3D printing dendrite-free lithium anodes based on the nucleated MXene arrays[J]. Energy Storage Materials, 2020, 24: 670-675.

[76] Luo J M, Zhang W K, Yuan H D, et al. Pillared structure design of MXene with ultralarge interlayer spacing for high-performance lithium-ion capacitors[J]. ACS Nano, 2017, 11(3): 2459-2469.

[77] Luo J M, Wang C L, Wang H, et al. Pillared MXene with ultralarge interlayer spacing as a stable matrix for high performance sodium metal anodes[J]. Advanced Functional Materials, 2019, 29(3): 1805946.

[78] Tang J, Peng X, Lin T, et al. Confining ultrafine tin monophosphide in $Ti_3C_2T_x$ interlayers for rapid and stable sodium ion storage[J]. eScience, 2021, 1(2): 203-211.

[79] Pu J, Li J, Shen Z, et al. Interlayer lithium plating in Au nanoparticles pillared reduced graphene oxide for lithium metal anodes[J]. Advanced Functional Materials, 2018, 28(41): 1804133.

[80] Yan K, Lu Z, Lee H W, et al. Selective deposition and stable encapsulation of lithium through heterogeneous seeded growth[J]. Nature Energy, 2016, 1(3): 16010.

[81] Qian Y, Wei C, Tian Y, et al. Constructing ultrafine lithiophilic layer on MXene paper by sputtering for stable and flexible 3D lithium metal anode[J]. Chemical Engineering Journal, 2021, 421: 129685.

[82] Gu J, Zhu Q, Shi Y, et al. Single zinc atoms immobilized on MXene ($Ti_3C_2Cl_x$) layers toward dendrite-free lithium metal anodes[J]. ACS Nano, 2020, 14(1): 891-898.

[83] Tian Y, An Y, Wei C, et al. Flexible and free-standing $Ti_3C_2T_x$ MXene@Zn paper for dendrite-free aqueous zinc metal batteries and nonaqueous lithium metal batteries[J]. ACS Nano, 2019, 13(10): 11676-11685.

[84] Shen Y, Pu Z, Zhang Y, et al. MXene/ZnO flexible freestanding film as a dendrite-free support in lithium metal batteries[J]. Journal of Materials Chemistry A, 2022, 1(33): 17199-1727.

[85] Na Z, Li W, Li L, et al. Conductive iodine-doped red phosphorus enabled dendrite-free lithium deposition on MXene matrix[J]. Small, 2022, 18(48): 2204341.

[86] Zhang W, Jin H, Du Y, et al. Sulfur and nitrogen codoped Nb_2C MXene for dendrite-free lithium metal battery[J]. Electrochimica Acta, 2021, 390: 138812.

[87] Wei C, Fei H, Tian Y, et al. Isotropic Li nucleation and growth achieved by an amorphous liquid metal nucleation seed on MXene framework for dendrite-free Li metal anode[J]. Energy Storage Materials, 2020, 26: 223-233.

[88] Zhu M, Xu K, Li D, et al. Guiding smooth Li plating and stripping by a spherical island model for lithium metal anodes[J]. ACS Applied Materials & Interfaces, 2020, 12(34): 38098-38105.

[89] Oyakhire S T, Huang W, Wang H, et al. Revealing and elucidating ALD-derived control of lithium plating microstructure[J]. Advanced Energy Materials, 2020, 10(44): 2002736.

[90] Luan J, Zhang Q, Yuan H, et al. Sn layer decorated copper mesh with superior lithiophilicity for stable lithium metal anode[J]. Chemical Engineering Journal, 2020, 395: 124922.

[91] Luo J M, Tao X Y, Zhang J, et al. Sn^{4+} ion decorated highly conductive Ti_3C_2 MXene: Promising lithium-ion anodes with enhanced volumetric capacity and cyclic performance[J]. ACS Nano, 2016, 10(2): 2491-2499.

[92] Luo J M, Lu X, Matios E, et al. Tunable MXene-derived 1D/2D hybrid nanoarchitectures as a stable matrix for dendrite-free and ultrahigh capacity sodium metal anode[J]. Nano Letters, 2020, 20(10): 7700-7708.

[93] Liu Y, Sun C, Lu Y, et al. Lamellar-structured anodes based on lithiophilic gradient enable dendrite-free lithium metal batteries with high capacity loading and fast-charging capability[J]. Chemical Engineering Journal, 2023, 451: 138570.

[94] Wang C Y, Zheng Z J, Feng Y Q, et al. Topological design of ultrastrong MXene paper hosted Li enables ultrathin and fully flexible lithium metal batteries[J]. Nano Energy, 2020, 74: 104817.

[95] Qian X, Fan X, Peng Y, et al. Polysiloxane cross-linked mechanically stable MXene-based lithium host for ultrastable lithium metal anodes with ultrahigh current densities and capacities[J]. Advanced Functional Materials, 2021, 31(6): 2008044.

[96] Zhao Z, Li B. Multi-storey corridor structured host for a large area capacity and high rate metallic lithium anode[J]. Electrochimica Acta, 2021, 365: 137341.

[97] Shao J J, Lv W; Yang Q H. Graphene: Self-assembly of graphene oxide at interfaces[J]. Advanced Materials, 2014, 26(32): 5732-5732.

[98] Zhang X, Lv R, Wang A, et al. MXene aerogel scaffolds for high-rate lithium metal anodes[J]. Angewandte Chemie, 2018, 57(46): 15028-15033.

[99] Fang Y, Zhang Y, Zhu K, et al. Lithiophilic three -dimensional porous $Ti_3C_2T_x$-rGO membrane as a stable scaffold for safe alkali metal (Li or Na) anodes[J]. ACS Nano, 2019, 13(12): 14319-14328.

[100] Shi H, Zhang C J, Lu P, et al. Conducting and lithiophilic MXene/graphene framework for high-capacity, dendrite-free lithium –metal anodes[J]. ACS Nano, 2019, 13(12): 14308-14318.

[101] Shi H, Yue M, Zhang C J, et al. 3D flexible, conductive, and recyclable $Ti_3C_2T_x$ MXene-melamine foam for high-areal-capacity and long-lifetime alkali-metal anode[J]. ACS Nano, 2020, 14(7): 8678-8688.

[102] Guo D, Ming F, Shinde D B, et al. Covalent assembly of two-dimensional COF-on-MXene heterostructures enables fast charging lithium hosts[J]. Advanced Functional Materials, 2021,

31(25): 2101194-n/a.

[103] Wang J, Yang M, Zou G, et al. Lithiation MXene derivative skeletons for wide-temperature lithium metal anodes[J]. Advanced Functional Materials, 2021, 31(21): 2101180.

[104] Zhao F, Zhai P, Wei Y, et al. Constructing artificial SEI layer on lithiophilic MXene surface for high-performance lithium metal anodes[J]. Advanced Science, 2022, 9(6): 2103930.

[105] Huang T, Xiong W, Ye X, et al. Constructing robust polymer/two-dimensional $Ti_3C_2T_x$ solid-state electrolyte interphase via in-situ polymerization for high-capacity long-life and dendrite-free lithium metal anodes[J]. Journal of Colloid and Interface Science, 2022, 628: 583-594.

[106] Lee S H, Kim M S, Lee J-H, et al. A Li-In alloy anode and Nb_2CT_x artificial solid-electrolyte interphase for practical li metal batteries[J]. Journal of materials chemistry A, 2022, 10(8): 4157-4169.

[107] Lagadec M F, Zahn R; Wood V. Characterization and performance evaluation of lithium-ion battery separators[J]. Nature Energy, 2019, 4(1): 16-25.

[108] Zhang Y, Yang G, Lehmann M L, et al. Separator effect on zinc electrodeposition behavior and its implication for zinc battery lifetime[J]. Nano Letters, 2021, 21(24): 10446-10452.

[109] Hao H, Hutter T, Boyce B L, et al. Review of multifunctional separators: Stabilizing the cathode and the anode for alkali (Li, Na, and K) metal –sulfur and selenium batteries[J]. Chemical Reviews, 2022, 122(9): 8053-8125.

[110] Li Y, Gao T, Ni D, et al. Two birds with one stone: Interfacial engineering of multifunctional janus separator for lithium–sulfur batteries[J]. Advanced Materials, 2022, 34(5): 2107638.

[111] Zhou W, Chen M, Tian Q, et al. Cotton-derived cellulose film as a dendrite-inhibiting separator to stabilize the zinc metal anode of aqueous zinc ion batteries[J]. Energy Storage Matarials, 2022, 44: 57-65.

[112] Zhao Q, Zhou R, Wang C, et al. Anion immobilization enabled by cation-selective separators for dendrite-free lithium metal batteries[J]. Advanced Functional Materials, 2022, 32(23): 2112711.

[113] Han X, Chen J, Chen M, et al. Induction of planar Li growth with designed interphases for dendrite-free Li metal anodes[J]. Energy Storage Materials, 2021, 39: 250-258.

[114] Wen J, Huang L, Huang Y, et al. A lithium-MXene composite anode with high specific capacity and low interfacial resistance for solid-state batteries[J]. Energy Storage Materials, 2022, 45: 934-940.

[115] Kumar B, Scanlon L G, Spry R J. On the origin of conductivity enhancement in polymer-ceramic composite electrolytes[J]. Journal of Power Sources, 2001, 96(2): 337-342.

[116] Pan Q, Zheng Y, Kota S, et al. 2D MXene-containing polymer electrolytes for all-solid-state lithium metal batteries[J]. Nanoscale Advances, 2019, 1(1): 395-402.